Received 23 December 2023; Accepted 18 February 2024
https://doi.org/10.48612/letters/2024-1-72-78

Chemically controlled radiation resistance of single-phase fcc Ni-Fe-Cr concentrated solid solutions

A. V. Korchuganov[†,1,2], O. A. Berezikov[1,2]

[†]avkor@ispms.ru

[1]Institute of Strength Physics and Materials Science of Siberian Branch of Russian Academy of Sciences, Tomsk 634055, Russia
[2]Tomsk State University, Tomsk 634050, Russia

Abstarct: The role of chemical composition in governing the radiation resistance mechanisms of fcc Ni-Fe-Cr concentrated solid solutions was studied using molecular dynamics simulation. The structural response of a material to irradiation is greatly influenced by the content of specific chemical elements. The main characteristics of defects formed by single atomic displacements cascades are calculated. The number of survived point defects decreases with a decrease in the Cr fraction and an increase in the Fe fraction in the Ni-Fe-Cr composition. The degree of clustering of interstitial atoms and the maximum size of their clusters decrease with increasing Fe and Cr content. An increase in the Fe fraction enhances the clustering of vacancies and increases the size of their clusters. Features of defect clustering in single cascades determine the evolution of the defect structure during prolonged irradiation (hundreds of cascades), which allows the development of high-level models based on low-level data. By tuning the chemical composition of the material, it is possible to achieve the formation of a certain defect structure with an optimal spatial distribution and number of interstitial dislocation loops and vacancy defects, which will effectively interact with each other, leading to self-healing of radiation damage during prolonged irradiation.

Keywords: concentrated solid solution, atomic displacement cascade, point defect clusters, dislocation loop, molecular dynamics

1. Introduction

The search for new concepts and methods for creating promising structural and functional materials with increased radiation resistance for use in nuclear energy is one of the key and most topical challenges of modern materials science [1–4]. This requires a fundamental understanding of the processes that occur in materials under harsh conditions of radiation exposure.

Primary radiation damage, which determines the further structural response of the material to irradiation, begins at the atomic level [5,6]. When neutrons or ions collide with atoms of a material, atomic displacement cascades are generated in it. They represent a sequence of displacements of atoms from crystal lattice sites, leaving the so called "survived" point defects that form clusters. Diffusion and coalescence of these defect clusters leads to the formation of voids and dislocation loops, the accumulation and growth of which results in degradation of the material's performance characteristics.

Recently, qualitatively new results in studying the structural response of materials to irradiation have been achieved for single-phase concentrated solid solutions (CSSs) based on Ni, showing high radiation tolerance [2,7–9]. Mainly, this is due to the fundamental difference in the chemical composition of CSSs and traditional alloys. CSSs are disordered substitutional solid solutions of 2–5 chemical elements, in which the fraction of each element is tens of percent. As recent experimental and simulation studies show, the high chemical disorder of CSSs significantly affects the size, diffusion and interaction of point defect clusters and dislocation loops generated during irradiation [3,4,10]. It is shown in [10] that the diffusion of interstitial atoms in NiFe, NiCo and NiCoCr is chemically heterogeneous: migration occurs through atoms of one or two chemical elements, for which the formation energy of an interstitial atom has the smallest value. It was shown in [3,11] that atomic displacement cascades generate a smaller number of defects in CSSs compared to pure metal.

In laboratory conditions, materials are typically irradiated with high-energy ions. Such effect on single-phase CSSs with an fcc structure leads to the formation of stacking fault tetrahedra (SFT) and voids from vacancies and dislocation loops from interstitial atoms [9,11–13]. A TEM study of the structure of Ni and Ni-based CSSs irradiated with 1.5 and 3 MeV Ni^+ ions was carried out in [9]. It was found that Ni and NiCo contain large voids closer to the surface, and an interstitial dislocation network is formed at greater depths. The NiFe, NiCoFe, NiCoFeCr and NiCoFeCrMn samples had much smaller voids. *In-situ* TEM studies have shown that the mobility of dislocation loops decreases with increasing number of chemical elements [13]. The highest loop mobility was for Ni, and lower for NiCo, NiFe and NiCoFeCr. At the same time, along with the chemical complexity of CSSs, the content of certain chemical elements has no less influence on the mobility of the loops [13,14]. Thus, elucidating the mechanisms that determine the features of the formation and

accumulation of radiation damage in the CSSs is a topical scientific problem. Therefore, the aim of this article is to study the influence of the chemical composition of the Ni-Fe-Cr CSSs on the features of the generation and accumulation of radiation defects during ion irradiation.

2. Materials and methods

The study was carried out within the framework of computer simulation in the LAMMPS software package [15] based on the molecular dynamics method. The method used is the most effective for simulation of primary radiation damage, since it allows one to explicitly take into account the atomic structure and chemical heterogeneity of the CSSs, and to study in detail the dynamics of material's structural changes during irradiation. To describe the interaction between atoms in the Ni-Fe-Cr system, a many-body potential was used [16], constructed within the framework of the embedded atom method. It accurately describes lattice parameters, elastic moduli, energies of formation, binding and migration of point defects, structural features and energy parameters of extended defects, which is important for correct simulation of CSS irradiation. The results of calculations of the above characteristics using this potential are in good agreement with experimental data and *ab-initio* calculations [16,17]. Due to the fact that the potential smoothly transforms into a screened Coulomb potential, it correctly describes the interaction of atoms at distances less than 1 Å, at which atoms approach each other during the development of high-energy atomic displacement cascades. The applicability of this potential for more correct simulation of atomic displacement cascades was demonstrated in [16]. To identify point defects in the irradiated material, an algorithm was used to analyze the occupancy of Wigner-Seitz cells, which were constructed for atoms at the sites of the initial crystal lattice. If the Wigner-Seitz cell does not contain atoms in an irradiated crystallite, then it is considered a vacancy; if it contains two or more atoms, then each subsequent atom after the first is considered a self-interstitial atom (SIA). It was considered that point defects constitute one cluster if each defect in the cluster is located at a distance of the second coordination sphere from at least one other defect in the cluster. Cluster size was calculated as the number of defects in cluster. To classify dislocation lines, the Dislocation Extraction Algorithm was used [18]. The described algorithms are implemented in the OVITO software package [19], which was used to analyze and visualize the structure of the simulated samples.

Two series of calculations were carried out: simulation of single atomic displacement cascades and simulation of prolonged irradiation of samples. To ensure the stability of the fcc structure of the simulated CSSs, the range of Fe and Cr concentrations was limited to values from 0 to 50%. In order to study in detail the influence of each chemical element, the fractions of Fe and Cr atoms in the simulated samples were 0, 0.1, 0.2, 0.33, 0.4, 0.5 with the condition that the fraction of Ni was not lower than 0.33. The choice of such values of Fe and Cr concentrations made it possible to form a uniform grid of points on the ternary diagrams and to interpolate the values of the calculated properties for intermediate concentrations. Based on this condition, 19 chemical compositions of CSSs, listed in Table S1 (supplementary material), as well as pure Ni, were considered for simulation of single cascades, and compositions $Ni_{40}Fe_{10}Cr_{50}$, NiFe and Ni were considered for simulation of prolonged irradiation. All samples were single crystals with an fcc lattice. The initial temperature of the samples was 900 K. To generate a cascade, one of the sample atoms was given a momentum corresponding to a kinetic energy of 20 keV.

When simulating single cascades, 20 calculations for each chemical composition were carried out with different directions of the primary knock-on atom momentum. The simulation time for each cascade was 2 ns. The samples had the shape of a cube with a side of 100 lattice parameters. Periodic boundary conditions were specified in all directions. When simulating prolonged irradiation, atomic displacement cascades were generated sequentially every 20 ps in the same sample. For the first 15 ps, the cascade was simulated in the NVE ensemble; for the remaining 5 ps, a thermostat was applied to the sample to rescale the temperature to 900 K. The total simulation time for each CSS was 14 ns, which corresponded to the formation of 700 cascades. The samples had dimensions of 300×100×100 lattice parameters along the X, Y, Z axes, respectively. Periodic boundary conditions were specified along the Y and Z axes, and free ones were applied along the X axis. To avoid surface effects and study the development of radiation damage in the bulk of the material, the cascade generation region was located at a distance of 70 lattice parameters from the free surfaces, allowing defects to freely migrate towards the free surface simulating sink. The size of this region was determined by the maximum distance traveled by displaced atoms during the generation of single cascades, increased by 20 lattice parameters.

3. Results and discussion

3.1. Single atomic displacement cascades

One of the most informative characteristics of a material's primary radiation damage is the number of stable point defects generated after the development of atomic displacement cascade. At the first stage of cascade development, the number of atoms displaced from lattice sites and corresponding number of Frenkel pairs increases. Then, the majority of atoms return to lattice sites and intense recombination of vacancies and SIAs occurs. At the end of this stage, the cascade "cools down" and "survived" point defects and their clusters are formed.

Stable configurations of survived defects formed after cooling down of displacement cascade will determine the degree of radiation damage of the material. Therefore, the influence of CSS chemical composition on the main characteristics of defects was studied in this work (Fig. 1, S1, S2). For visual convenience, the figures show smoothed contour graphs instead of separate points for each of the 20 compositions. As can be seen from Fig. 1a, the number of survived point defects decreases with a decrease in the Cr content and an increase in the fraction of Fe in the CSS, which is consistent with experimental and simulation data [11, 20]. The fraction of clustered SIAs is the same for compositions with a Fe content of more than 25%; for other

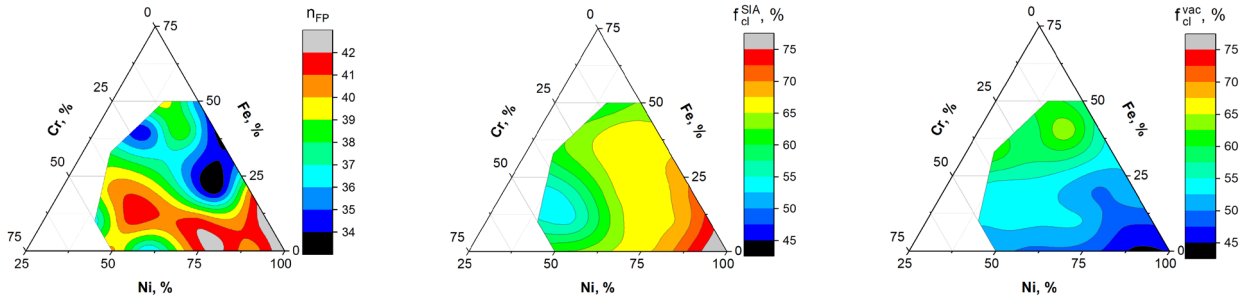

a b c

Fig. 1. (Color online) Number of survived Frenkel pairs (a); fraction of SIAs (b) and vacancies (c) forming clusters 20 ps after cascade generation in samples of different chemical compositions.

compositions it increases from ≈50 to 80% with increasing Ni content and decreasing Cr fraction (Fig. 1b). The fraction of clustered vacancies increases with increasing Fe content, and its effect is most pronounced at Cr concentrations less than 25% (Fig. 1c). A high degree of clustering (60 – 70%) for both vacancies and SIAs is observed in the upper part of the ternary diagram; in the lower left part it is less — 50 – 60%. For the lower right corner, there is a significant difference in the clustering of vacancies and SIAs. This difference is maximum in Ni: SIA clustering is almost two times higher than that of vacancies.

The distributions of SIAs and vacancies in clusters of different sizes are shown in Figs. S1 and S2, respectively (see supplementary material). To plot these dependencies, the number of defects in all clusters of a certain size was normalized to the total number of defects. For almost all compositions, majority of SIAs form clusters of sizes 2 – 11 (Fig. S1). In Ni, about half of the SIAs form clusters of sizes greater than 21. About a third of the vacancies primarily form clusters of sizes 2 – 11 for all compositions (Fig. S2). For compositions in which the fraction of vacancies in clusters of sizes 2 – 11 is lower than others, the fraction of vacancies in clusters of sizes greater than 21 is increased. These are compositions with a Cr content of less than 25% and Ni in the ranges of 40 – 50% or 70 – 80%.

The mechanism of formation of point defect clusters by atomic displacement cascades is the same for all compositions considered and is as follows. After reaching the maximum number of displaced atoms, the radiation-damaged region has a maximum volume. SIAs are formed at its periphery, and in its volume — the cascade core — the material is in a dynamic state close to a melt: its structure is close to a liquid, the atomic velocities correspond to temperatures of thousands of degrees, the atomic density is reduced (excess vacancies) [21]. This "molten" core then begins to cool down, and the structure in the damaged region crystallizes from the periphery to the center of the core. As the crystallization front moves, mono- and divacancies usually survive in the crystallized region. After crystallization of the core is complete, the largest cluster of vacancies remains at its center.

Our simulations showed that the larger the initial volume of the molten core of the cascade and the longer the time of its crystallization, the more single and divacancies are formed behind the crystallization front, and the smaller the cluster of vacancies remains in the center of this region after crystallization is completed. The correlation between the cooling time of the cascade and the fraction of vacancies that form clusters larger than 21 defects is evident from a comparison of Fig. S2 c and Fig. S3 (supplementary material). It can be seen that for most compositions, an increase in the Cr fraction and a decrease in the Fe fraction leads to an increase in the cooling time of the cascade and the formation of smaller vacancy clusters.

Mainly single SIAs are formed at the periphery of the radiation-damaged region. Since these defects are highly mobile, after reaching the maximum volume of the damaged region, they quickly form large and low-mobile clusters, which further do not interact with the rapidly cooling "molten" cascade core over the next 10 – 15 ps. The fraction of SIAs in clusters larger than 21 defects (Fig. S1c, supplementary material) correlates well with the mobility of a single SMA (Fig. S4): a comparison of the figures shows that with increasing Cr concentration, both the mobility of single SIA and the fraction of SIAs in clusters larger than 21 decrease.

Within 2 ns, majority of the single SIAs move significantly away from the region in which the atomic displacement cascade was formed. The diffusion path of a single SIA is longer for compositions with a lower Cr content and a higher Fe content, see Fig. S4 (supplementary material). NiFe is characterized by the maximum mobility of SIA, one of the lowest values is found in $Ni_{40}Fe_{10}Cr_{50}$. It can be assumed that the migration of point defects that have left the atomic displacement cascades that formed them will influence the mechanisms of formation of larger radiation defects during prolonged irradiation. Therefore, the above compositions with different mobility of SIA and Ni were chosen to study the characteristics of damage accumulation during prolonged irradiation. In addition to this, these compositions have significant differences in the clustering of defects formed by single cascades.

3.2. Prolonged irradiation

Let us consider the dependence of the number of survived point defects on the irradiation time as an integral parameter characterizing the radiation damage of a material (Fig. 2). This figure also shows linear dependences that approximate the total number of defects that would be formed during the same simulation time by atomic displacement cascades which are isolated from each other (i. e., every 20 ps the number of survived point defects for a single cascade from Fig. 1a was

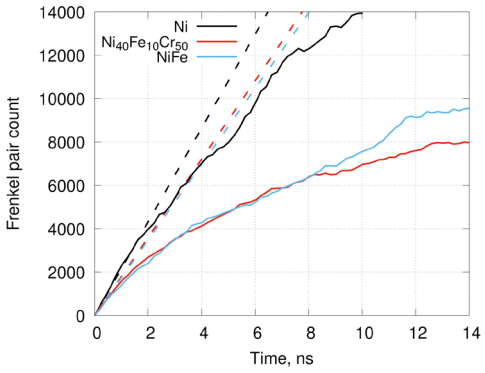

Fig. 2. (Color online) The number of survived point defects versus irradiation time for various chemical compositions of samples (solid lines) and the total number of defects formed by the same number of isolated cascades (dashed lines).

added). From a comparison of the linear approximations and the observed curves, it is clear that the deviation from isolated production of defects in cascades begins in the first nanoseconds. This indicates the activation of the mechanisms of point defect annihilation. It is due to not only the replacement of old defects by a new cascade, but also the interaction of formed defects. The rate of accumulation of the number of defects is almost two times lower, and the deviation from the linear dependence is stronger for the $Ni_{40}Fe_{10}Cr_{50}$ and NiFe compositions compared to Ni. After 8 ns, the number of defects begins to differ for $Ni_{40}Fe_{10}Cr_{50}$ and NiFe. The reasons for the above differences are related to the specifics of defect cluster formation in these materials, which will be discussed below.

As the radiation dose increases, the number of defects increases and clusters of larger sizes are formed (Fig. S5), and defects are also redistributed among clusters of different sizes. The spatial distribution of point defects in the samples is shown in Fig. S6. The change in the fraction of vacancies and SIAs in clusters of various sizes is shown in Figs. 3 and 4, respectively. The methodology for calculating histogram data is similar to that used for the single cascades in Figs. S1 and S2. In general, the fraction of single defects (which do not form clusters) in the total number of defects decreases and the fraction of SIAs in small clusters also decreases with time.

At the initial stage of irradiation, about 40% of vacancies are single for the compositions considered (Fig. 3). Their fraction decreases with time by about 10%. The fraction of vacancies in clusters with sizes up to 41, 61, 71 remains virtually unchanged for Ni, $Ni_{40}Fe_{10}Cr_{50}$ and NiFe, respectively, with the exception that there is a decrease for clusters with sizes 2–11 in NiFe. As the dose accumulates, new clusters with sizes larger than those indicated above begin to appear. At the same time, the maximum size of vacancy clusters in Ni is almost two times larger than the sizes for $Ni_{40}Fe_{10}Cr_{50}$ and NiFe; by 10 ns it is about 200 vacancies (Fig. S5 b).

The fraction of single SIAs is initially low and decreases significantly with time (Fig. 4). Already at 2 ns, the total fraction of SIAs in clusters larger than 41 in size in Ni is much higher compared to other compositions, and the fraction of SIAs in clusters of smaller sizes is lower (Fig. 4 a). As irradiation proceeds, the fraction of defects in clusters larger than 151 increases from 10 to 70%. This clustering rate is maximum for the compositions considered. This correlates with the results of studying clusters for single cascades in Ni: the fraction of SIAs in clusters and the sizes of these clusters are maximum for this material compared to the considered CSSs. Also from Fig. S5 a, one can see that the maximum size of the SIA cluster in Ni is an order of magnitude larger than for other compositions.

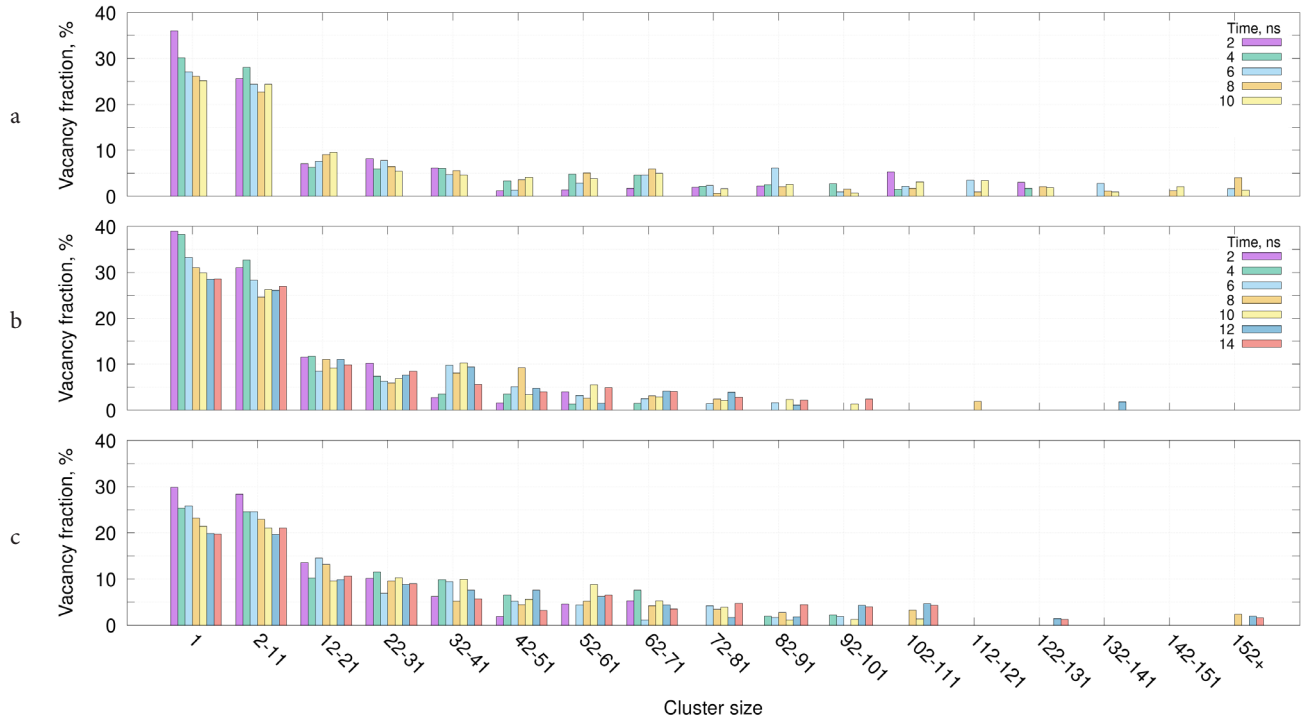

Fig. 3. (Color online) The fraction of vacancies in clusters of different sizes at different times for Ni (a), $Ni_{40}Fe_{10}Cr_{50}$ (b) and NiFe (c).

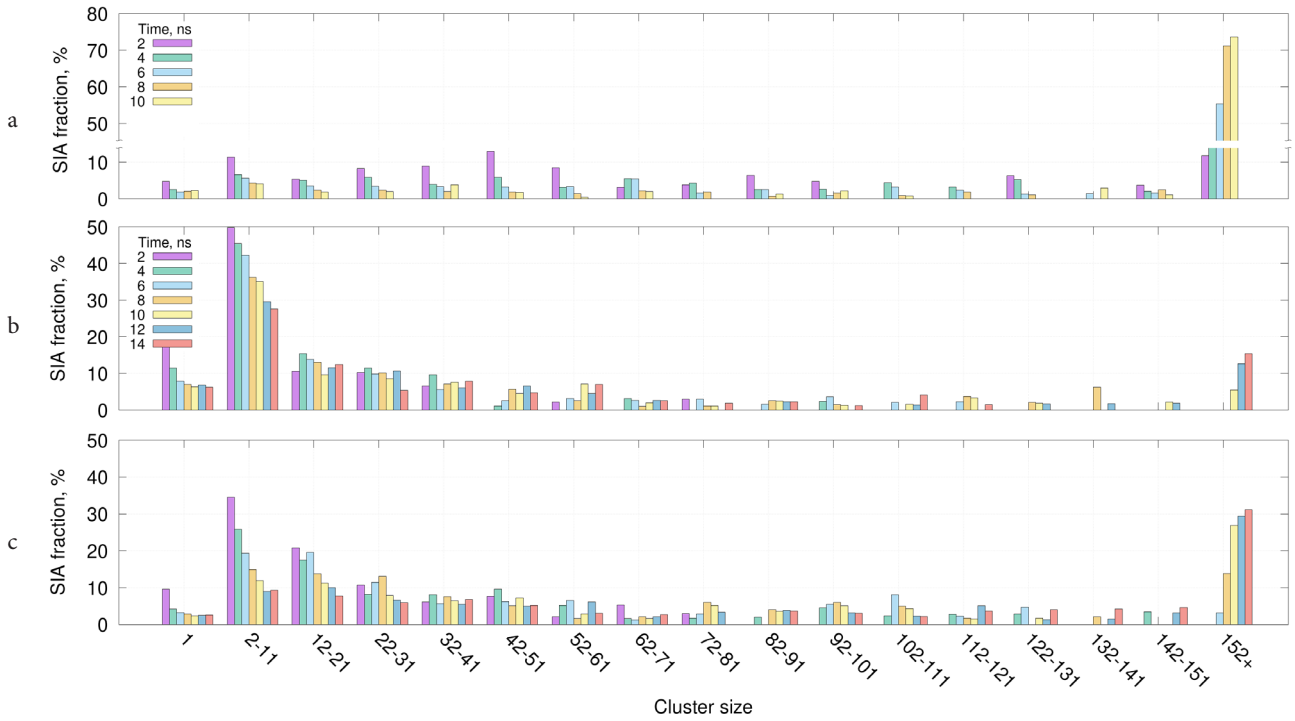

Fig. 4. (Color online) The fraction of SIAs in clusters of different sizes at different times for Ni (a), $Ni_{40}Fe_{10}Cr_{50}$ (b) and NiFe (c).

At the initial stage of irradiation of $Ni_{40}Fe_{10}Cr_{50}$ sample, about half of the defects are small clusters of sizes 2–11 (Fig. 5b). In the interval of 4–8 ns, clusters with sizes from 42 to 141 are actively formed, the fraction of defects in clusters with sizes 2–11 decreases. Further, in the interval of 8–12 ns, the fraction of clusters with size 2–11 continues to decrease and clusters larger than 151 SIAs appear.

In NiFe already at 2 ns there are more clusters with sizes greater than 41 than in $Ni_{40}Fe_{10}Cr_{50}$ and the average cluster size increases faster with time than in $Ni_{40}Fe_{10}Cr_{50}$ (Fig. 5c), the maximum cluster size also increases faster (Fig. S5a). In the interval of 6–10 ns, the fraction of SIAs in clusters with sizes larger than 151 sharply increases, and the fraction of defects in clusters with sizes up to 22 decreases significantly. In the interval of 10–14 ns, the fraction of defects in clusters with sizes 2–21 and 152+ does not change; the total fraction of defects in clusters with sizes 112–151 increases. The more intense formation of large SIA clusters, which turned out to be more stable, in NiFe compared to $Ni_{40}Fe_{10}Cr_{50}$ led to differences in the further dynamics of defect accumulation in the curve in Fig. 3. This correlates with the fact that for single cascades the NiFe composition is also more prone to the formation of large-sized clusters and the total fraction of clustered defects in it is higher than in $Ni_{40}Fe_{10}Cr_{50}$.

For all compositions considered, all SIA clusters with sizes larger than 10 are dislocation loops with different Burgers vectors. Vacancies form voids in nickel, SFT in $Ni_{40}Fe_{10}Cr_{50}$, and they can form both SFT and voids in NiFe. The dependences of the total length of dislocation lines on irradiation time are presented in Fig. 5. The dislocation structure of irradiated samples at different times is shown in Fig. S7.

Shockley 1/6<112> partial dislocations, bordering the intrinsic stacking faults, are the most numerous and longest in all samples. These dislocations make up the vast majority of segments on the split loops of full 1/2<110> dislocations. A similar structure of such loops was obtained in molecular dynamics simulations in [11].

In Ni, the total length of the 1/6<112> loops increases quite quickly (Fig. 5a), starting from 4 ns the loops reach relatively large sizes (Fig. 4a), become more mobile and actively combine into larger defects (Fig. S7a). Due to this, individual loops are contained in Ni in small quantities, but in large sizes. For example, three separate loops coalescence into one containing about 3000 SIAs in the time interval of 8–10 ns. The 1/3<111> interstitial loops are the second in total length in Ni, their length reaches saturation already at 2 ns. They border the extrinsic stacking faults and are sessile. During irradiation, these small loops can be annihilated by cascades, while larger ones virtually do not change their size. All clusters of more than 10 vacancies in Ni are voids.

The length of 1/6<112> dislocations in the $Ni_{40}Fe_{10}Cr_{50}$ sample is the maximum among the compositions (Fig. 5b), due to the fact that the sizes of individual dislocation loops are small, but their number is large. The mobility of such loops is lower than in Ni. In the time interval of 8–12 ns, large 1/6<112> loops appear (these are SIA clusters of size 152+ in Fig. 4b), which grow and become more mobile. At an interval of 12–14 ns, they begin to actively interact with each other and other defects, mainly by absorbing SFT. As a result, the growth rate of the defect number decreases (Fig. 2). Also the length of 1/6<110> stair-rod dislocations is maximal in $Ni_{40}Fe_{10}Cr_{50}$, which border the SFT consisting of vacancies. The dimensions and number of SFT are larger than in NiFe. More numerous and more homogeneously distributed clusters of defects of both vacancy and interstitial types in $Ni_{40}Fe_{10}Cr_{50}$ (for example, SIA loops and SFT) interact and

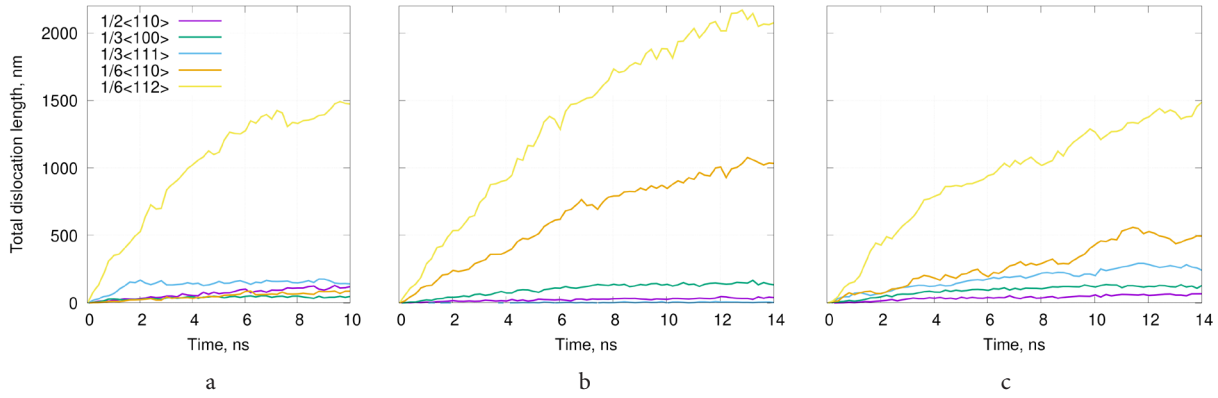

Fig. 5. (Color online) Total length of dislocations with different Burgers vectors versus irradiation time for Ni (a), $Ni_{40}Fe_{10}Cr_{50}$ (b) and NiFe (c).

annihilate more effectively, which leads to greater radiation resistance of the material compared to other compositions — the number of defects is minimal (Fig. 2).

1/6<112> loops in NiFe are contained in smaller amounts than in $Ni_{40}Fe_{10}Cr_{50}$ (Fig. 5c). At the same time, they are larger in size than in $Ni_{40}Fe_{10}Cr_{50}$. They are also smaller than in Ni, although the total length of dislocations in Ni and NiFe is the same. The length of 1/6<110> stair-rod dislocations, as well as the number of SFT bordered by them, is less than in $Ni_{40}Fe_{10}Cr_{50}$. From 9 to 11 ns, new SFT are more actively generated, but then their concentration decreases due to their absorption by 1/6<112> loops, which have combined into larger and more mobile defects. As a result, the growth rate of point defect number decreases. The total length of 1/3<111> dislocations slowly increases due to the nucleation of new small sessile loops.

Vacancy clusters can form both SFT and voids in NiFe. This variability is associated with the high chemical disorder of the CSS, it greatly affects the stacking fault energy [22] and locally determines the type of defect formed by vacancies. Being in a certain region of the sample with a specific local chemical composition, the cluster of vacancies remains either a SFT or a void and is not further transformed into another type. Since the strength of interaction between dislocation loops and vacancy defects of different types is different, the concentration of such defects will determine the rate of their annihilation.

4. Conclusions

In this work, using computer simulation by the molecular dynamics method, the features of point defect clustering in single atomic displacement cascades, as well as the features of the damage accumulation during prolonged irradiation were studied for Ni-Fe-Cr CSSs of different chemical compositions. It has been shown that a decrease in the fraction of Cr and an increase in the fraction of Fe in the Ni-Fe-Cr leads to a decrease in the number of survived point defects in the material. The addition of Fe and Cr to Ni reduces the degree of SIA clustering and the maximum size of clusters formed after cooling down of the atomic displacement cascade. An increase in the fraction of Fe for CSSs with a Cr content <25% enhances the clustering of vacancies and increases the size of their clusters.

The number of defects formed in CSSs during prolonged irradiation is much less than in Ni and significantly lower than the cumulative estimate based on the average number of defects generated by isolated cascades. The main mechanism of radiation resistance of Ni-Fe-Cr CSS is the annihilation of interstitial loops and SFT. It occurs most intensively in $Ni_{40}Fe_{10}Cr_{50}$ due to the optimal sizes of vacancy and interstitial defects and their most uniform distribution over the sample. Depending on the local chemical environment, either a void or a SFT can be formed by vacancies in NiFe. Thus, knowing the influence of the chemical composition on the stability of vacancy defects of a certain type, it becomes possible to vary their concentration and size in order to control the rates of reactions between them and interstitial loops. The features of radiation defect clustering during prolonged irradiation correlate well with the results for single cascades. Ni is more prone to the formation of large vacancy and SIA clusters, intermediate cluster sizes are observed in NiFe, and clusters in $Ni_{40}Fe_{10}Cr_{50}$ have the minimum sizes. Thus, data for single cascades can be used in higher-level models to predict the defect structure under prolonged irradiation of a material.

Supplementary material: *The online version of this paper contains supplementary material available free of charge at the journal's website (lettersonmaterials.com).*

Acknowledgements: *This work was supported by the grant of the President of the Russian Federation MK-5189.2022.1.2.*

References

1. G.S. Was, D. Petti, S. Ukai, S. Zinkle. J. Nucl. Mater. 527, 151837 (2019).
2. K. Jin, H. Bei. Front. Mater. 5, 26 (2018).
3. Y. Zhang, S. Zhao, W.J. Weber, K. Nordlund, F. Granberg, F. Djurabekova. Curr. Opin. Solid State Mater. Sci. 21, 221 (2017).
4. Z. Cheng, J. Sun, X. Gao, Y. Wang, J. Cui, T. Wang, H. Chang. J. Alloys Compd. 930, 166768 (2023).
5. K. Nordlund, S.J. Zinkle, A.E. Sand, F. Granberg, R.S. Averback, R.E. Stoller, T. Suzudo, L. Malerba, F. Banhart, W.J. Weber, F. Willaime, S.L. Dudarev, D. Simeone. J. Nucl. Mater. 512, 450 (2018).

6. K.P. Zolnikov, A.V. Korchuganov, D.S. Kryzhevich, V.M. Chernov, S.G. Psakhie. Phys. Mesomech. 22, 355 (2019).
7. M.-R. He, S. Wang, K. Jin, H. Bei, K. Yasuda, S. Matsumura, K. Higashida, I.M. Robertson. Scr. Mater. 166, 96 (2019).
8. C. Parkin, M. Moorehead, M. Elbakhshwan, J. Hu, W.Y. Chen, M. Li, L. He, K. Sridharan, A. Couet. Acta Mater. 198, 85 (2020).
9. C. Lu, L. Niu, N. Chen, K. Jin, T. Yang, P. Xiu, Y. Zhang, F. Gao, H. Bei, S. Shi, M.-R. He, I.M. Robertson, W.J. Weber, L. Wang. Nat. Commun. 7, 13564 (2016).
10. S. Zhao, Y. Osetsky, Y. Zhang. Acta Mater. 128, 391 (2017).
11. C. Shan, L. Lang, T. Yang, Y. Lin, F. Gao, H. Deng, W. Hu. Comput. Mater. Sci. 177, 109555 (2020).
12. C. Lu, K. Jin, L.K. Béland, F. Zhang, T. Yang, L. Qiao, Y. Zhang, H. Bei, H.M. Christen, R.E. Stoller, L. Wang. Sci. Rep. 6, 19994 (2016).
13. S. Shi, H. Bei, I.M. Robertson. Mater. Sci. Eng. A. 700, 617 (2017).
14. D. Utt, S. Lee, Y. Xing, H. Jeong, A. Stukowski, S.H. Oh, G. Dehm, K. Albe. Nat. Commun. 13, 4777 (2022).
15. S. Plimpton. J. Comput. Phys. 117, 1 (1995).
16. L.K. Béland, A. Tamm, S. Mu, G.D. Samolyuk, Y.N. Osetsky, A. Aabloo, M. Klintenberg, A. Caro, R.E. Stoller. Comput. Phys. Commun. 219, 11 (2017).
17. Interatomic Potentials Repository. Available online (accessed on 1 Feb. 2024).
18. A. Stukowski, V.V. Bulatov, A. Arsenlis. Model. Simul. Mater. Sci. Eng. 20, 085007 (2012).
19. A. Stukowski. Model. Simul. Mater. Sci. Eng. 18, 015012 (2010).
20. K. Jin, W. Guo, C. Lu, M.W. Ullah, Y. Zhang, W.J. Weber, L. Wang, J.D. Poplawsky, H. Bei. Acta Mater. 121, 365 (2016).
21. A.F. Calder, D.J. Bacon, A.V. Barashev, Yu.N. Osetsky. Philos. Mag. 90, 863 (2009).
22. S. Zhao, Y. Osetsky, G.M. Stocks, Y. Zhang. npj Comput. Mater. 5, 13 (2019).